GT2018-75692

ADJOINT METHODS FOR ELIMINATION OF THERMOACOUSTIC OSCILLATIONS IN A MODEL ANNULAR COMBUSTOR VIA SMALL GEOMETRY MODIFICATIONS

José G. Aguilar *
Department of Engineering
University of Cambridge
Cambridge, United Kingdom CB21PZ
Email: jga28@cam.ac.uk

Matthew P. Juniper
Department of Engineering
University of Cambridge
Cambridge, United Kingdom CB21PZ
Email: mpj1001@cam.ac.uk

ABSTRACT

In gas turbines, thermoacoustic oscillations grow if moments of high fluctuating heat release rate coincide with moments of high acoustic pressure. The phase between the heat release rate and the acoustic pressure depends strongly on the flame behaviour (specifically the time delay) and on the acoustic period. This makes the growth rate of thermoacoustic oscillations exceedingly sensitive to small change in the acoustic boundary conditions, geometry changes, and the flame time delay. In this paper, adjoint-based sensitivity analysis is applied to a thermoacoustic network model of an annular combustor. This reveals how each eigenvalue is affected by every parameter of the system. This information is combined with an optimization algorithm in order to stabilize all thermoacoustic modes of the combustor by making only small changes to the geometry. The final configuration has a larger plenum area, a smaller premix duct area and a larger combustion chamber volume. All changes are less than 6% of the original values. The technique is readily scalable to more complex models and geometries. This demonstrates why adjoint-based sensitivity analysis and optimization could become an indispensible tool for the design of thermoacoustically-stable combustors.

NOMENCLATURE

A duct area
c speed of sound
k flame interaction index
L duct length
m mass flux
n azimuthal wave number
p pressure
Q heat release
r radius
R duct mean radius
t time
u axial velocity
v radial velocity
w azimuthal velocity
x axial position
$(\bar{\ })$ mean quantities
$(\hat{\ })$ perturbation quantities
$(\ )^+$ adjoint variables
γ ratio of specific heat capacities
δ small quantities
θ azimuthal angle
λ growth rate
ρ density
σ angular frequency
τ time delay
ω eigenvalue
$\mathscr{J}$ cost function
$\mathscr{L}$ Lagrangian functional

---

*Address all correspondence to this author.

INTRODUCTION

If heat release rate fluctuations in gas turbine combustion chambers occur in phase with acoustic pressure fluctuations, then heat is converted to work and the acoustic amplitude grows. The heat release rate is large (often several megawatts), so this thermodynamic process needs to be only slightly efficient for the amplitude of acoustic oscillations to become large. These thermoacoustic oscillations produce noise and mechanical vibrations. They are one of the most persistent and challenging problems facing gas turbine and rocket engine manufacturers [1].

Thermoacoustic oscillations are usually eliminated by a combination of modelling, trial and error experimental testing, and addition of passive control devices such as Helmholtz resonators. Configurations that are thought to be stable after engine component tests often turn out to be unstable during full engine tests [2]. At this stage, it is possible to perform several full engine tests on slightly different configurations until one is found that is stable across the entire operating regime [3]. Usually, however, this is prohibitively expensive. It is more common to add passive control methods, such as acoustic liners, Helmholtz resonators, quarter and half wave tubes, baffles etc. [4]. These exploit vortex shedding and viscous losses to add acoustic damping at selected frequencies. Their major drawback is that the damped frequency range can be quite narrow and they are usually unable to adjust to different operating conditions.

Another option is feedback control. This has been shown to be effective in laboratory combustors [5]. It has the advantage that it can readily adapt to changes in the operation conditions but the disadvantage that it relies on the effectiveness of the sensors and actuators, which must operate without fault for several million cycles. Another approach is to tune passive control devices so that their effective frequency range can be adapted to the operating conditions. For example [6] and [7] tuned Helmholtz resonators and acoustic liners by varying their geometry, neck area or pipe length respectively. Both of these methods introduce new failure modes into systems that must usually be designed to be safe and reliable. This is undesirable and these methods are usually avoided.

Thermoacoustic systems are exceedingly sensitive to small changes [8] and can usually be stabilized by making only small changes. The ideal approach is therefore to tweak the shape of the system until a stable configuration is achieved. The challenge is to identify these small changes before the full engine test stage. In this study we identify every unstable thermoacoustic mode and use adjoint methods [9] to calculate their sensitivities to all geometry changes. We then combine this with an optimization routine that stabilizes all of these thermoacoustic modes by slightly modifying the geometry. Any stable modes that become unstable are also targeted and stabilized. The advantage of this approach is that, unlike a Helmholtz resonator, it stabilizes all unstable frequencies. The disadvantage is that it relies on an accurate model of the real system (a disadvantage shared by all other methods),

the consequences of which we will discuss in the conclusions.

1 LOW ORDER NETWORK MODELLING

Thermoacoustic oscillations in combustion chambers tend to have relatively long wavelengths compared to the flow features and can therefore be modelled reasonably accurately with acoustic network models. In this paper we follow the approach developed by Stow and Dowling [10–12], to model a thin annular combustor. In this type of model, travelling acoustic and convective waves propagate through and interact with ducts, combustion zones and boundary conditions. The major assumption is that short zones, such as the combustion zone, are acoustically compact [13]. To model an annular combustor with a ring of premix ducts, different approaches can be used [14, 15]. In this paper, however, we follow the model provided by Stow and Dowling [12].

1.1 Governing equations

The low order network model is developed in cylindrical polar coordinates with governing equations for mass, momentum and energy, assuming no viscosity or heat conduction:

$$\frac{\partial \rho}{\partial t} + \nabla \cdot (\rho u_t) = 0, \tag{1a}$$

$$\rho \frac{\partial u_t}{\partial t} + \rho (u_t \cdot \nabla) u_t + \nabla p = 0, \tag{1b}$$

$$\frac{\partial p}{\partial t} + u_t \cdot \nabla p + \gamma p \nabla \cdot u_t = (\gamma - 1) Q, \tag{1c}$$

where $u_t = (u, v, w)^T$ represents the velocities in the x, r and θ directions, ρ is the density, p is the pressure, Q is the heat addition, and γ is the ratio of specific heat capacities, which here is assumed constant.

Many industrial applications involve combustors in which the radial gap is shorter than the axial length and much shorter than the circumference. Under these conditions it is common to set $v = 0$ and to neglect all variations in the radial (r) direction [11]. This is the narrow gap approximation.

Following the formalism developed by Stow and Dowling [10] we linearise the governing equations around a steady and uniform base flow, which varies only in the axial direction. The flow variables take the form $p = \bar{p}(x) + p'(x, \theta, t)$ and $\bar{w} = 0$ [11]. We then perform a Fourier transform in θ and t such that the perturbations become $p'(x, \theta, t) = \hat{p}(x) e^{i\omega t + in\theta}$ with complex frequency ω and azimuthal wave number n.

1.2 Network Modules

The network is composed of ducts connected by modules representing jump conditions such as an area increase, area decrease, heat sources and boundary conditions.

1.2.1 Ducts The fundamental elements in low order network modelling are straight ducts. For a thin annular configuration, these are characterised by a cross sectional area A, length L, and mean radius $R = (r_1 + r_2)/2$, where r_1 and r_2 are the inner and outer radii of the annular gap. The ducts have homogeneous properties and are governed by the linearised Euler equations. These form a convected wave equation, whose solutions are four travelling waves: two acoustic waves that propagate at the speeds $\bar{c} \pm \bar{u}$ (where $\bar{c}$ is the mean speed of sound) and two convective waves (representing entropy and vorticity waves) that propagate at the mean flow speed $\bar{u}$.

1.3 Jump conditions

Annular combustors often contain a ring of premix ducts where the fuel is injected. To model this we follow [12], where conservation of quantities is enforced in a sector of the annulus and then integrated over the entire ring. At the start of the premix ducts, mass flux, entropy, and energy flux are conserved, while the angular momentum is assumed to be zero. The former is true because the premix ducts are considered as one dimensional elements where only plane waves propagate. At the end of the premix ducts the combustion chamber is modelled again as a thin annulus. In this jump the conserved fluxes are mass, angular momentum, and energy, while the axial momentum flux is increased by the pressure of the walls. This approach sets a restriction on the maximum azimuthal wave number used, which is less than half of the number of premix ducts in the configuration [12, 15] Finally, the heat release is modelled in the combustion chamber by assuming conservation of mass, axial momentum, and angular momentum fluxes, while the energy flux is increased by the added heat release. For this section the unsteady heat release is modelled with a mass-driven $n - \tau$ model:

$$\frac{\hat{Q}}{\bar{Q}} = k \frac{\hat{m}_x}{\bar{m}_x} e^{-i\omega\tau}, \tag{2}$$

where Q is the heat release, k the interaction index, $m = A\rho u$ the mass flux, and τ is the time delay. The subscript denotes the quantities at position x in the premix ducts. Note that the unsteady heat source model is proportional to the unsteady mass flow rate at position x in the premix duct but it's independent of its angle, therefore, circumferential modal coupling is not introduced into the system [12]. Kinematic flame models [16–18] and flame transfer function analysis such as [19] suggest that the interaction index and the time delay should be modelled as functions of the Strouhal number which depends on the flow and the duct area. However, to keep the thermoacoustic model as simple as possible those will be treated as constants.

1.4 Boundary conditions

The model also requires a set of boundary conditions at the inlet and outlet. Annular configurations often have a compressor at the inlet and a turbine at the outlet, which can be acoustically modelled with closed ends ($\hat{u} = 0$), with reflection coefficients or more conveniently as choked ends. For our model we use the acoustically choked ends described in [20].

1.5 The eigenvalues

The thermoacoustic network model is created by stacking the preceding elements one behind the other. In this paper, the eigenvalues are found by guessing an initial value for ω at the inlet boundary and then propagating the acoustic wave through the network until the exit boundary condition is reached. The value of ω is then updated, using a Newton-Raphson method, until the exit boundary condition is satisfied.

2 ADJOINT BASED SENSITIVITY ANALYSIS

In this paper, the sensitivity of each eigenvalue to all possible configuration changes is calculated with a single adjoint calculation. Adjoint methods were first applied to thermoaoustic systems by Magri and Juniper [9], using Galerkin methods for the acoustics. They were extended to wave based thermoacoustic systems by Aguilar et al. [21].

In general, there are two families of adjoint methods: the continuous adjoint, in which one derives and solves the adjoint of the continuous governing equations, and the discrete adjoint, in which one solves the adjoint of the discretized equations. In this paper, we use the continuous approach, which allows us to include base flow modifications more easily. We follow the adjoint based sensitivity analysis developed in [21] to compute the sensitivities to the areas, lengths, and mean radii of the ducts as well as to the flame parameters. Finally, we use these information as an input to an optimization routine used to stabilize all of the resonant modes in a given configuration.

2.1 The adjoint equations

To obtain the adjoint equations we first create a Lagrangian functional. Taking $[\cdot, \cdot]$ as an appropriate inner product, the functional becomes:

$$\mathscr{L} \equiv \omega - \left[\hat{q}^+, P(\omega, \hat{q}, G)\right] - \left[G^+, B(G)\right], \tag{3}$$

where ω is the eigenvalue. The first inner product is between the Lagrange multipliers, $\hat{q}^+$, and the perturbation equations and jump conditions, P, which in turn depend on the eigenvalue, the perturbation variables, $\hat{q}$, and the base flow quantities, G. The second inner product is between the Lagrange multipliers, G^+,

and the equations of the steady problem given by the steady jump conditions, B, which depend on the base flow variables, G.

Following a continuous adjoint approach we use the first inner product to compute the adjoint perturbation equations for each of the elements in the network. We then use the full functional to compute the adjoint base flow equations, which are used to compute the variation of the eigenvalue whenever a change to one of the parameters also affects the base flow.

2.1.1 Adjoint equations for ducts.

Here we present the adjoint equations for the ducts in order to show the symmetry between the direct and the adjoint equations, and to give a brief insight into the elements used to compute the sensitivities. Following [21], to obtain the adjoint equations we take the derivative of the Lagrangian functional with respect to the perturbation variables $(\hat{p}, \hat{\rho}, \hat{u}, \hat{w})$. After integration by parts this produces the adjoint equations. First we present the unsteady adjoint equations and then the corresponding steady adjoint equations.

For a straight duct, the relevant components of vector P in Eq. 3 are given by the linearised form of Eqs. 1. Their corresponding adjoint variables or Lagrange multipliers (components of vector $\hat{q}^+$) are given by the spatial functions $(\hat{\rho}^+(x), \hat{u}^+(x), \hat{w}^+(x), \hat{p}^+(x))^T$ respectively. The resulting adjoint perturbation equations are:

$$i\omega^*\hat{\rho}^+ + \bar{u}\frac{d\hat{\rho}^+}{dx} = 0, \qquad (4a)$$

$$i\omega^*\bar{\rho}\hat{u}^+ + \bar{\rho}\bar{u}\frac{d\hat{u}^+}{dx} + \bar{\rho}\frac{d\hat{\rho}^+}{dx} + \gamma\bar{p}\frac{d\hat{p}^+}{dx} = 0, \qquad (4b)$$

$$i\omega^*\bar{\rho}\hat{w}^+ + \frac{in}{R}\bar{\rho}\hat{\rho}^+ + \frac{in}{R}\gamma\bar{p}\hat{p}^+ + \bar{\rho}\bar{u}\frac{d\hat{w}^+}{dx} = 0, \qquad (4c)$$

$$i\omega^*\hat{p}^+ + \bar{u}\frac{d\hat{p}^+}{dx} + \frac{in}{R}\hat{w}^+ + \frac{d\hat{u}^+}{dx} = 0. \qquad (4d)$$

The boundary terms are:

$$\left[\left(\hat{\rho}^{+*}\bar{u}\right)\delta\bar{\rho} + \left(\hat{\rho}^{+*}\bar{\rho} + \hat{u}^{+*}\bar{\rho}\bar{u} + \hat{p}^{+*}\gamma\bar{p}\right)\delta\hat{u} + \cdots\right.$$
$$\left.\left(\hat{u}^{+*} + \hat{p}^{+*}\bar{u}\right)\delta\hat{p} + \left(\hat{w}^{+*}\bar{\rho}\bar{u}\right)\delta\hat{w}\right]_{x_0}^{x_1} = 0, \qquad (5)$$

where the locations x_0 and x_1 are the positions of the inlet and outlet of the duct. The boundary terms must be zero for arbitrary perturbations (δ terms), so the terms in brackets must be zero. These terms are used to compute the adjoint jump conditions and adjoint boundary conditions.

As for the direct equations, the adjoint equations can be decoupled into a set of four adjoint waves: two adjoint acoustic waves, and two adjoint convective waves. The adjoint eigenvalues are the complex conjugates of the direct eigenvalues [9].

For a straight duct, the relevant components of vector B in Eq. 3 are given by the steady part of Eqs. 1. The corresponding Lagrange multipliers (components of vector G^+) are given by the spatial functions $(R^+(x), U^+(x), W^+(x), P^+(x))^T$ respectively. The resulting adjoint base flow equations are given by:

$$\bar{u}\frac{dR^+}{dx} = -i\omega^*(\hat{w}^*\hat{w}^+ + \hat{u}^*\hat{u}^+) - \frac{in}{R}\hat{w}^*\hat{\rho}^+ + \cdots$$
$$\bar{u}\hat{w}^+\frac{d\hat{w}^*}{dx} + \left(\hat{\rho}^+ + \bar{u}\hat{u}^+\right)\frac{d\hat{u}^*}{dx}, \qquad (6a)$$

$$\bar{\rho}\frac{dR^+}{dx} + \bar{\rho}\bar{u}\frac{dU^+}{dx} + \gamma\bar{p}\frac{dP^+}{dx} = \hat{\rho}^+\frac{d\hat{\rho}^*}{dx} + \cdots$$
$$\bar{\rho}\hat{w}^+\frac{d\hat{w}^*}{dx} + \bar{\rho}\hat{u}^+\frac{d\hat{u}^*}{dx} + \hat{p}^+\frac{d\hat{p}^*}{dx}, \qquad (6b)$$

$$\frac{dU^+}{dx} + \bar{u}\frac{dP^+}{dx} = \gamma\hat{p}^+\left(-\frac{in}{R}\hat{w}^* + \frac{d\hat{u}^*}{dx}\right), \qquad (6c)$$

$$\frac{dW^+}{dx} = 0, \qquad (6d)$$

The corresponding boundary terms are:

$$\left[\left(R^+\bar{u}\right)\delta\bar{\rho} + \left(R^+\bar{\rho} + U^+\bar{\rho}\bar{u} + P^+\gamma\bar{p}\right)\delta\bar{u} + \cdots\right.$$
$$\left.W^+\delta\bar{w} + \left(U^+ + \bar{u}P^+\right)\delta\bar{p}\right]_{x_0}^{x_1} = 0. \qquad (7)$$

Whenever x_0 or x_1 represents a position of the duct where there are fixed properties, such as at the boundaries, this implies that their corresponding δ terms are zero. For example, if the pressure is fixed at the inlet, then at that location $\delta\bar{p} = 0$, since the value of $\bar{p}$ lies outside of the computational domain [22]. The remaining terms should still equate to zero to obtain the corresponding sensitivities at the inlet boundary condition. If there are no fixed properties the steady boundary terms work similarly as in the unsteady case. Note that the adjoint steady flow equations use the solution of the adjoint unsteady flow equations.

2.2 Sensitivity analysis

To calculate the sensitivities of an eigenvalues with respect to all parameters, we follow the method in [21]. We set the derivative of the Lagrangian with respect to the desired parameter, A, to zero: $\partial\mathcal{L}/\partial A = 0$. For this, knowledge of the direct and adjoint variables is required. For the annular combustor the geometric parameters of interest are the length of the ducts, the areas, mean radii and the time delay of the heat source. The time delay is included because it is easily influenced by the fuel injector design and is also one of the most influential parameters in a thermoacoustic system [8].

3 OPTIMIZATION

An application of adjoint based shape optimization in aero-acoustics can be seen in [23]. In that study the geometry of the neck of a Helmholtz resonator was optimized to obtain a desired impedance. In a different manner, our application aims to stabilize all of the thermoacoustic unstable modes of the system. This is one of the multiple requirements in the gas turbine industry, which include reduction of emmisions, optimization of fuel consupmtion, performance, durability, serviceability, etc. [24].

3.1 Optimization routine

The adjoint-based sensitivity analysis described in §2 gives the gradient of each eigenvalue with respect to the geometric parameters. These gradients can be used in a gradient descent algorithm. Our aim is to stabilize all of the thermoacoustic modes of an annular combustor simultaneously and we must allow for unstable modes to disappear or re-appear during the optimization process. Therefore, we follow the following steps:

1. Compute the resonant thermoacoustic modes of the system (the eigenvalues).
2. Compute the sensitivity of the eigenvalues with respect to the geometric parameters (A, L, R, τ).
3. Given a set of constraints and maximum allowed displacements, use an optimization algorithm to compute the changes in the parameters such that the cost function (below) is optimally reduced.
4. Update the configuration and iterate until all the modes are stable.

3.2 The cost function and optimization algorithm

By introducing a small change to one of the system's parameters (denoted by δA), the eigenvalues shift. The predicted eigenvalue Ω_j is given by: $\Omega_j = \omega_j + \delta \omega_j$, where ω_j is an eigenvalue of the system, and $\delta \omega_j$ is the corresponding eigenvalue drift, which is given by the sum of the sensitivities:

$$\delta \omega_j = \sum_{k=1}^{N_X} \frac{\partial \omega_j}{\partial A_k} \delta A_k, \qquad (8)$$

where N_X is the number of relevant parameters in the system. In the studied frequency range the system will have N_ω resonant modes, each of them represented by: $\omega_j = \sigma_j - i\lambda_j$ where σ is the angular frequency and λ is the growth rate. Our objective is to stabilize all of the resonant modes (i.e., $\lambda_j < 0$ for j = 1, ..., N_ω) by introducing small changes into the system. To ensure that all the modes are stabilized we set an objective growth rate λ_o such that $\lambda_o \leq 0$. Once a mode reaches this objective we will not seek to stabilize it further. With this information we build a predictor function $\Psi_j(\delta A)$. This function gives 0 if a mode is stable or the

growth rate plus the shift if the mode is unstable:

$$\Psi_j(\delta A) = \begin{cases} \Phi_j(\delta A) & \text{if } \Phi_j(\delta A) > 0, \\ 0 & \text{if } \Phi_j(\delta A) < 0, \end{cases}$$

$$\Phi_j(\delta A) = \underbrace{\lambda_j + \sum_{k=1}^{N_X} \frac{\partial \lambda_j}{\partial A_k} \delta A_k}_{-\text{Im}\{\Omega_j(\delta A)\}} - \lambda_o.$$

The reduced version of the cost function $\mathscr{J}(\delta A)$, which we minimize, is then given by the sum of the predictor functions over all of the eigenvalues of the system.

By setting the objective growth rate to be $\lambda_0 \leq -1$ we can further add a small constraint to the cost function in order to select the parameters that produce the smallest variations in the configuration. By considering δA_{m_k}, the maximum allowed change of the kth parameter the cost function becomes:

$$\underbrace{\mathscr{J}(\delta A) = \sum_{j}^{N_\omega} \Psi_j(\delta A)}_{\text{Reduced version}} + \frac{1}{N_x} \sum_{k=1}^{N_X} \frac{|\delta A_k|}{\delta A_{m_k}}. \qquad (9)$$

Whenever all the modes are stable, the first summation in the cost function is zero so the algorithm seeks the configuration that requires the smallest change. In order to compute the the changes in the parameters that minimize the cost function, we use a barrier method. The constrained minimization problem becomes:

$$\begin{aligned} &\text{minimize} && \mathscr{J}(\delta A) \\ &\text{subject to} && -\delta A_{m_k} \leq \delta A_k \leq \delta A_{m_k}, && k = 1, ..., N_X \end{aligned}$$

where δA_{m_k} is given as a small percentage of the parameter's value.

4 APPLICATION
4.1 Annular combustor model

The annular combustor geometry in this paper is the same as that in [25]. The geometry is shown in Figs. 1 and 2. It consists of a thin annular plenum, followed by a ring of 20 premix ducts, and an annular combustion chamber. At the inlet the flow is choked and has a pressure of 5 bar, a temperature of 1000 K and a mass flow rate of 100 kg/s. In order to closely match the results reported in [25], we considered that (i) the flame is at rest, i.e. there is no moving flame front, and (ii) the combustion zone has a steady heat input of $\bar{Q} = 151.1$ MW, with interaction index of $k = -4$, and time delay of $\tau = 1.5 \times 10^{-3}$ s. At the outlet of the combustion chamber there is another choked end.
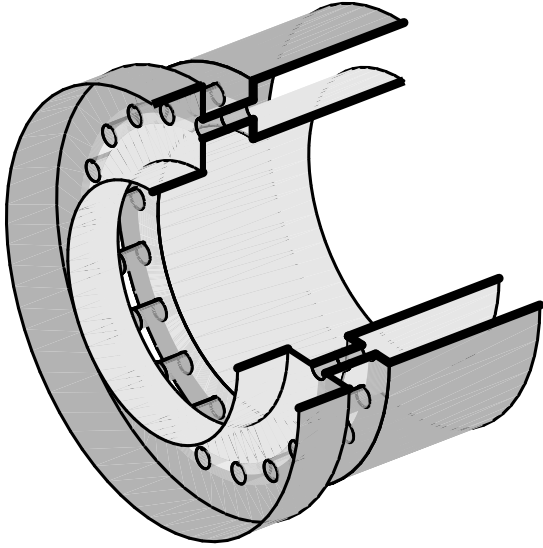
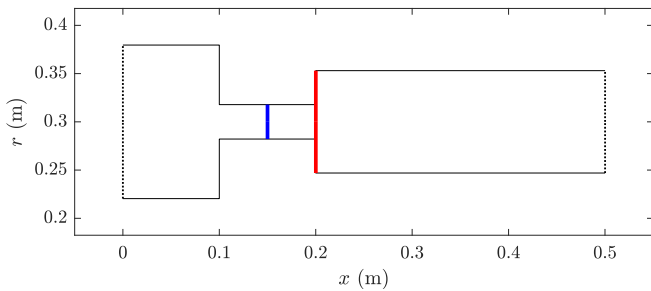**FIGURE 1**: 3D model of the annular combustor with a cross sectional cut.

FIGURE 2: 2D schematic of the annular combustor. The dotted lines at the inlet and outlet represent choked ends, the blue line represents the reading point of the heat source and the red line represents the flame position.

4.2 The eigenvalues

Given that the system is linear and that we are not introducing elements that break the symmetry of the configuration, such as Helmholtz resonators [26], the system will not present circumferential modal coupling. At first sight, we need to consider all possible azimuthal wave numbers n, where n is an integer. However, for high values of n the modes are strongly stable and do not need to be stabilized further. For the optimization routine, the highest azimuthal wave number we consider is $n = |3|$. This is less than the maximum $|n|$ imposed by the model, which has the constraint that $|n| < D/2$ where D is the number of premix ducts [12].

For frequencies up to 1000 Hz, Fig. 3 shows the error of the boundary condition at the outlet of the annular combustor for azimuthal wave numbers $n = 0$ and $n = \pm 1$. Eigenvalues

(white circles) are located where this error tends to zero. All of the eigenvalues at higher azimuthal wave numbers are stable (not shown here). For $n = 0$ (plane waves) there is an unstable mode at 57 Hz. For $n = \pm 1$ (first helical mode) there is an unstable mode at 547 Hz, which is very close to the one reported in [25]. The difference between the unstable modes reported in [25] and the present paper are due to the convective waves. In their model they are assumed to be zero, which is not true for ours.
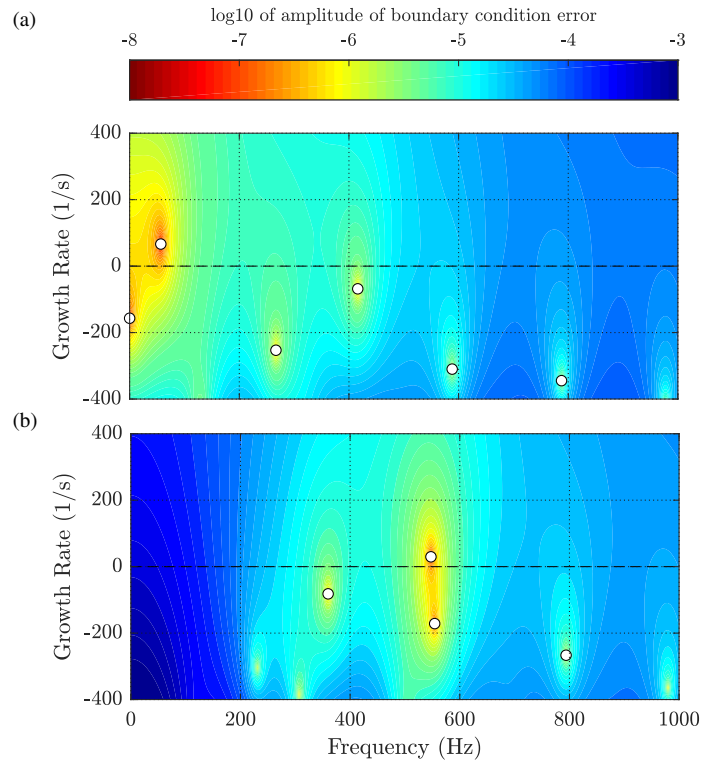

FIGURE 3: Plots of the boundary condition error for the initial configuration of the annular combustor. The white markers represent resonant modes (eigenvalues) found with the shooting method. (a) corresponds to azimuthal wave number $n = 0$ and (b) to $n = \pm 1$.

4.3 Sensitivity analysis

Before starting the optimization algorithm, it is worth commenting on the sensitivities of the initial configuration to changes in the relevant parameters. From Fig. 4, we see that the sensitivity to area change is one order of magnitude larger than the sensitivity to length and two orders of magnitude larger that the sensitivity to mean radius. This suggests that area changes will dominate the overall stabilization routine. This is because variations in area induce changes in the mean flow parameters and

6

hence the eigenvalues.

From Fig. 4a we see that the sensitivity to the area of the premix ducts is positive, which means that we expect the optimization routine to reduce this area. On the other hand, the sensitivity to the area of the plenum and combustion chamber is negative, which means that we expect the routine to increase these areas. From Fig. 4b, we see that the sensitivity to the length of the plenum is positive, so we expect it to reduce. The sensitivity to the length of the premix duct and the combustion chamber is negative, so we expect them to increase. Note that the sensitivity to the length of the premix duct is different on either side of the measurement point. From Fig. 4c, we see that the sensitivity to the mean radius is strongest in the combustion chamber, where we expect the mean radius to increase. From figure 5 we observe that the sensitivity of the time delay is at least one order of magnitude larger than any of the previous parameters. Furthermore, we note that while the sensitivity of the unstable modes points in the same direction (increase to stabilize), the majority of the stable modes point in the opposite direction. Given how sensitive the time delay is, and the lack of a preferred direction, in order to stabilize the system we expect minor changes in this parameter.

The sensitivities calculated with this adjoint method are compared with those calculated with a finite difference method for a handful of shifts in a given parameter's value. We check that the difference between the adjoint sensitivity and the finite difference sensitivity increases in proportion to the square of the shift in the parameter value. This is a strong test that the adjoint sensitivity is exact to first order and quickly reveals any defects in the adjoint derivation or adjoint code.

4.4 Geometry modifications for stability

Thermoacoustic oscillations are exceedingly sensitive to small changes in parameters and there are several ways to stabilize all of the eigenvalues by changing the geometry. In this paper, we examine five test cases. Each test case allows one or more geometric parameters to vary until the system is completely stable. The flame time delay τ is included because this is the convection time of the fuel injection process and is easily altered by changing the fuel injector. The test cases are:

Case 1: Variations in areas.
Case 2: Variations in areas and mean radius.
Case 3: Variations in areas and lengths.
Case 4: Variations in areas, lengths and mean radius.
Case 5: Variations in areas, lengths, mean radius and time delay.

In order to ensure a smooth variation of the geometric parameters, the maximum allowed change for each of the parameters is set as 0.1% of the current magnitude of the parameter. The target growth rate is set to $\lambda_o = -5/s$.
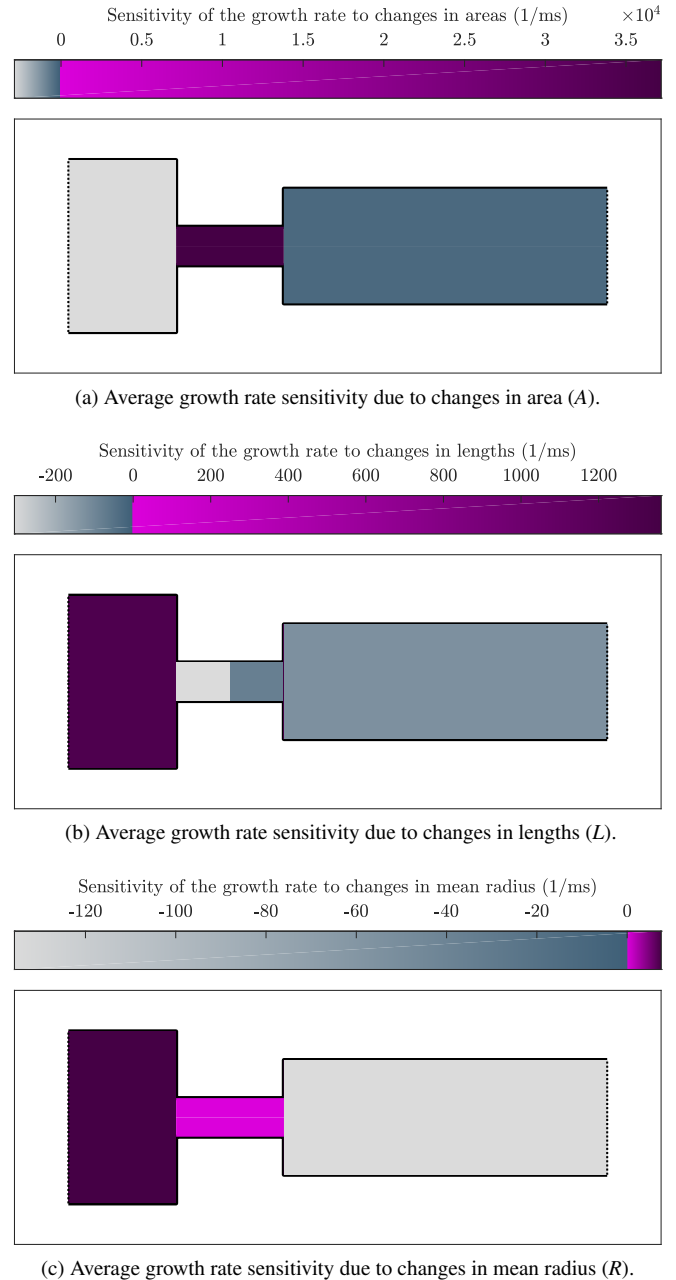

(a) Average growth rate sensitivity due to changes in area (*A*).

(b) Average growth rate sensitivity due to changes in lengths (*L*).

(c) Average growth rate sensitivity due to changes in mean radius (*R*).

FIGURE 4: Average growth rate sensitivity maps for the unstable modes of the annular combustor.

4.5 Results and discussion

From the boundary error plot in Fig. 3 we see that there are three resonant modes (one each for $n = 0$, $n = +1$, and $n = -1$). They have relatively small growth rates so we expect that only small changes will be required to stabilize the system. From Fig. 3b we further note that the eigenvalues are symmetric in *n*, which means that when all the unstable modes are included in
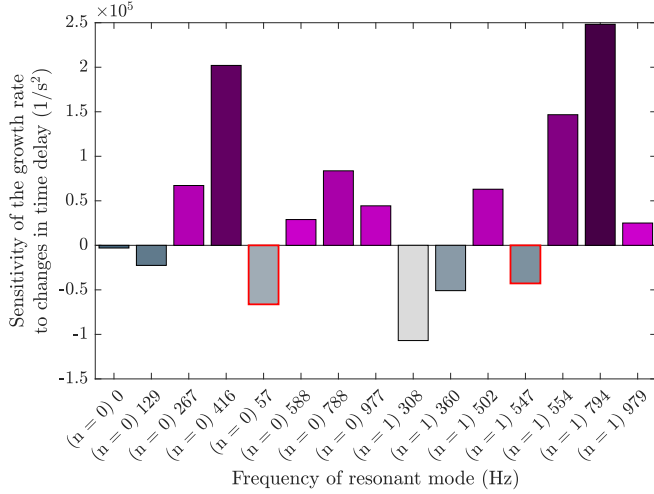
FIGURE 5: Sensitivity of the growth rates to changes in the time delay for all the resonant modes with azimuthal number $n = 0$ and $n = 1$. The red box denotes an unstable mode.

the cost function Eq. 9, the system will prioritize the stability of the circumferential modes ($|n| > 1$) because they will be present twice.

The initial (unstable) and final (stable) configurations are shown in Fig. 6. The corresponding eigenvalue trajectories for case 4 are shown in Fig. 7. The trajectories for the other cases are similar.

For case 1 (area variations only) we observe from Fig. 6a, that the predictions from the sensitivity analysis of the initial configuration are correct - i.e. that the largest area change is in the area of the premix ducts. The total area of the premix ducts reduces by 6.1% (i.e., the variation of a single premix duct as the one shown in the figure is 0.305%), the plenum increases by 4.7% and the combustion chamber increases by 3.2%.

Case 2 (area and mean radius variations) is shown in Fig. 6b. The mean radius of the plenum and premix ducts remain almost unchanged. The biggest area change is observed at the plenum with an increase of 5.6% followed by the premix ducts with a reduction of 5.2% and finally the combustion chamber with an increase of 1.8%.

In case 3 (length and area variations), the length of the plenum shrinks by 1.6% with respect to the original value, while the combustion chamber increases by 1.6% and the premix ducts increase only marginally.

For case 4 (variations in areas, lengths and mean radius) we see that changes in areas are more dominant, followed by variations in lengths and the mean radius.

The final case (variations in area, length mean radius and time delay) is not shown here because it has almost the same final configuration as case 4. The optimization routine finds a configuration in which the time delay changes only by $4 \times 10^{-5}\%$ with respect to the original value.

In general, we observe an increase in the area of the plenum, a reduction in the area of the premix ducts and an increase in the volume of the combustion chamber.

In all the test cases the aim is to optimize the geometry to achieve stability, based on a given operating condition. However, in industrial applications the opposite case is often the problem: find an stable operational map for a given geometry. In such cases the obvious test case would be to tune the parameters of the flame transfer function until a stable configuration is achieved. For the particular problem presented in this paper the tunable parameters would be the interaction index and the time delay. Given the behaviour of the time delay (see Fig. 5) the stable operational map would point towards reducing the interaction index. However, this parameter is hardly tunable and hence the best option would be to reformulate the flame transfer function in terms of parameters that can be changed (i.e., fuel flow rate, equivalence ratio, etc.).

It is worth mentioning that there will be many ways to stabilize this system. Different optimization procedures and different initial starting points would converge to different final configurations. In practice, a global optimization routine should be used.

5 CONCLUSIONS

In this study we successfully combine an adjoint-based sensitivity analysis with an optimization routine in order to passively stabilize a model of an annular combustion chamber by slightly changing its geometry.

We use a low order network model of an annular combustor with a ring of premix ducts. We derive the continuous adjoint equations and from these obtain the sensitivities of an eigenvalue to all geometric parameters. We create an optimization routine that can stabilize all eigenvalue simultaneously by tweaking the geometry. In this study, no new unstable modes appear. Even if they did appear, the optimization routine would stabilize them. The outcome is a set of different configurations which are completely stable within the selected frequency range.

By performing an analysis in the initial configuration, we are able to predict many of the trends that the final configurations will undergo. The final configuration has a larger plenum area, a smaller premix duct area and a larger combustion chamber volume. All changes are less than 6% of the original values.

This is the first study of adjoint-based geometry optimization of an annular combustion chamber. It shows that the process is remarkably efficient at stabilizing the eigenmodes of a thermoacoustic network model. Only small changes are required and, by employing a global optimization routine, it is likely that a stable configuration could be found with even smaller changes. These proposed changes are preferable to the addition of passive devices such as Helmholtz resonators, which add weight, cost, and complexity.
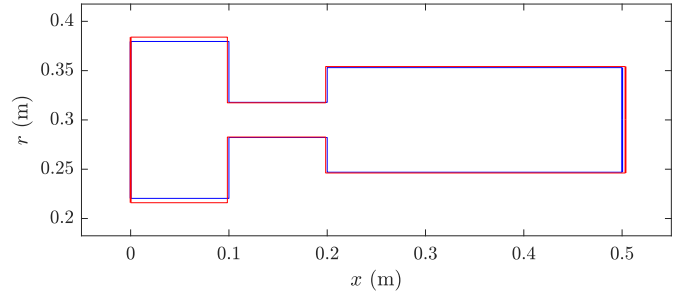
8
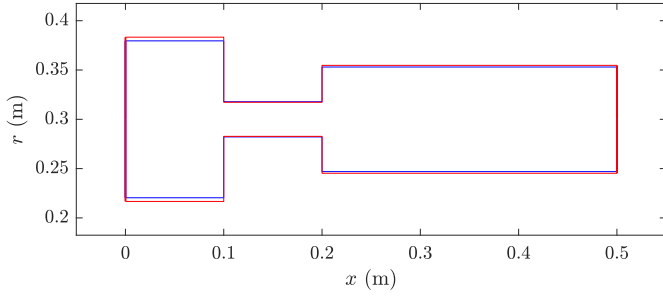
(a) Case 1: variations in areas (A). The change in area with respect to the original magnitudes are: plenum: 4.7%, premix ducts: -6.1% total (-0.305% single), combustion chamber: 3.2%.
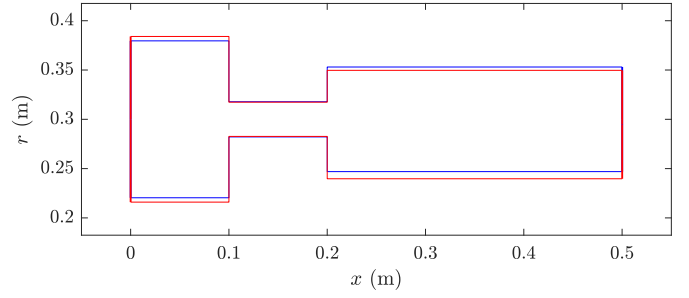
(b) Case 2: variations in areas (A) and mean radius (R). The change in area with respect to the original magnitudes are: plenum: 5.6%, premix ducts: -5.2% total (-0.26% single), combustion chamber: 1.8%. The change in mean radius with respect to the original magnitudes are: plenum: 0.0071%, premix ducts: 0.0071%, combustion chamber: -1.8%.
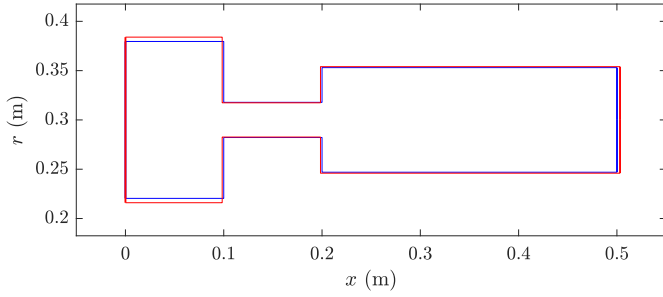
(c) Case 3: variations in areas (A) and lengths (L). The change in area with respect to the original magnitudes are: plenum: 5.5%, premix ducts: -5.3% total (-0.265% single), combustion chamber: 1.8%. The change in length with respect to the original magnitudes are: plenum: -1.6%, premix ducts: 4.9×10^{-4}%, combustion chamber: 1.6%.

(d) Case 4: variations in areas (A), lengths (L) and mean radii (R). The change in area with respect to the original magnitudes are: plenum: 5.5%, premix ducts: -5.3% total (-0.265% single), combustion chamber: 1.8%. The change in length with respect to the original magnitudes are: plenum: -1.6%, premix ducts: -1.5×10^{-4}%, combustion chamber: 1.6%. The change in mean radius with respect to the original magnitudes are: plenum: 1.5×10^{-4}%, premix ducts: -1.3×10^{-4}%, combustion chamber: 0.053%.

FIGURE 6: Cross section cut comparing the initial (blue) and final (red) configurations of the annular combustor after all the eigenvalues have been stabilized.

Adjoint-based sensitivity analysis and optimization could become an indispensible tool for the design of thermoacoustically-stable combustors. It is easy to add other constraints, either by adapting the cost function or by preventing the algorithm from entering regions of the design space. The next steps are to examine network models of more complex configurations with different heat release models, in particular those that can be compared with experiments. More complex systems have more parameters that can be varied. It is likely that more complex systems will be stabilized with smaller changes than those shown in this study.

Finally, it is worth noting that thermoacoustic systems can be stabilized with small geometry modifications because thermoacoustic oscillations are exceedingly sensitive to small changes. This means that any model of a system is severely prone to systematic error in the measurement of its parameters. It is useful that adjoint-based sensitivity analysis reveals the most influential parameters. This also highlights, however, that experiments are required to ensure that the model, on which the sensitivity analysis is based, is a fair reflection of reality. Experimental validation of eigenvalue sensitivity analysis on simple systems has been performed by [27–29]. Next steps will be to repeat this on more complex systems and to check the validity of the model's predictions.
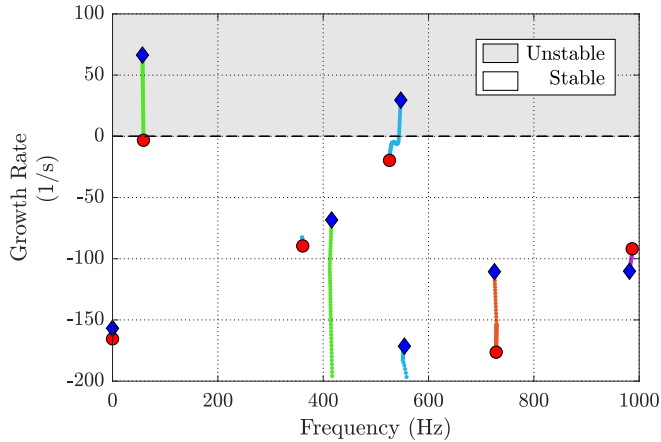
ACKNOWLEDGMENT

FIGURE 7: Eigenvalue trajectories from the initial (unstable) to the final (stable) configurations for variations in area, length and mean radii (Case 4). The other cases behave similarly. The blue diamonds (◇) represent the eigenvalues of the initial configuration and the red circles (○) represent the eigenvalues of the final configuration. The green, blue, orange and purple trajectories represent the eigenvalues for the azimuthal wave numbers $n = 0, n = \pm1, n = \pm2$ and $n = \pm3$ respectively.

REFERENCES

[1] Lieuwen, T. C., and Yang, V., eds., 2005. *Combustion instabilities in gas turbine engines: operational experience, fundamental mechanisms, and modeling*. AIAA.

[2] Mongia, H. C., Held, T. J., Hsiao, G. C., and Pandalai, R. P., 2003. "Challenges and progress in controlling dynamics in gas turbine combustors". *Journal of Propulsion and Power, 19*(5), pp. 822–829.

[3] Oefelein, J. C., and Yang, V., 1993. "Comprehensive Review of Liquid-Propellant Combustion Instabilities in F-1 Engines". *Journal of Propulsion and Power, 9*(5), pp. 657–677.

[4] Zhao, D., and Li, X., 2015. "A review of acoustic dampers applied to combustion chambers in aerospace industry". *Progress in Aerospace Sciences, 74*, apr, pp. 114–130.

[5] Dowling, A. P., and Morgans, A. S., 2005. "Feedback control of combustion oscillations". *Annual Review of Fluid Mechanics, 37*(1), pp. 151–182.

[6] Zhao, D., and Morgans, A. S., 2009. "Tuned passive control of combustion instabilities using multiple Helmholtz resonators". *Journal of Sound and Vibration, 320*(4-5), pp. 744–757.

[7] Zhao, D., Morgans, A. S., and Dowling, A. P., 2011. "Tuned Passive Control of Acoustic Damping of Perforated Liners". *AIAA Journal, 49*(4), pp. 725–734.

[8] Juniper, M. P., and Sujith, R. I., 2018. "Sensitivity and nonlinearity in Thermoacoustics". *Annual Review of Fluid Mechanics, 50*, pp. xxx—-xxx.

[9] Magri, L., and Juniper, M. P., 2013. "Sensitivity analysis of a time-delayed thermo-acoustic system via an adjoint-based approach". *Journal of Fluid Mechanics, 719*, pp. 183–202.

[10] Stow, S. R., and Dowling, A. P., 2001. "Thermoacoustic oscillations in an annular combustor". *ASME Turbo Expo*, pp. 2001–GT–0037.

[11] Dowling, A. P., and Stow, S. R., 2003. "Acoustic analysis of gas turbine combustors". *Journal of Propulsion and Power, 19*(5), pp. 751–764.

[12] Stow, S. R., and Dowling, A. P., 2004. "Low-order modelling of thermoacoustic limit cycles". *ASME Turbo Expo*.

[13] Dowling, A. P., 1995. "The calculation of thermoacoustic oscillations". *Journal of Sound and Vibration, 180*(4), mar, pp. 557–581.

[14] Bauerheim, M., Parmentier, J. F., Salas, P., Nicoud, F., and Poinsot, T., 2014. "An analytical model for azimuthal thermoacoustic modes in an annular chamber fed by an annular plenum". *Combustion and Flame, 161*(5), pp. 1374–1389.

[15] Evesque, S., and Polifke, W., 2002. "Low-order acoustic modelling for annular combustors: validation and inclusion of modal coupling". *ASME Conference Proceedings*(February), pp. 1–11.

[16] Fleifil, M., Annaswamy, A. M., Ghoneim, Z. A., and Ghoniem, A. F., 1996. "Response of a laminar premixed flame to flow oscillations: A kinematic model and thermoacoustic instability results". *Combustion and Flame, 106*(4), pp. 487–510.

[17] Dowling, a. P., 1999. "A kinematic model of a ducted flame". *Journal of Fluid Mechanics, 394*, pp. 51–72.

[18] Lieuwen, T., 2003. "Modeling premixed combustion-acoustic wave interactions: A review". *Journal of Propulsion and Power, 19*(5), pp. 765–781.

[19] Yi, T., and Santavicca, D. A., 2009. "Forced Flame Response of Turbulent Liquid-Fueled Lean-Direct-Injection Combustion to Fuel Modulations". *Journal of Propulsion and Power, 25*(6), nov, pp. 1259–1271.

[20] Stow, S. R., Dowling, A. P., and Hynes, T. P., 2002. "Reflection of Circumferential Modes in a Choked Nozzle". *Journal of Fluid Mechanics, 467*(x), pp. 1–25.

[21] Aguilar, J. G., Magri, L., and Juniper, M. P., 2017. "Adjoint-based sensitivity analysis of low-order thermoacoustic networks using a wave-based approach". *Journal of Computational Physics, 341*, jul, pp. 163–181.

[22] Marquet, O., Sipp, D., and Jacquin, L., 2008. "Sensitivity analysis and passive control of cylinder flow". *Journal of Fluid Mechanics, 615*, nov, pp. 221–252.

[23] Caeiro, F., Sovardi, C., Förner, K., and Polifke, W., 2017. "Shape optimization of a Helmholtz resonator using an adjoint method". *International Journal of Spray and Combustion Dynamics, 9*(4), dec, pp. 394–408.

[24] Lieuwen, T. C., and Yang, V., 2013. *Gas Turbine Emis-*

sions. Cambridge University Press.

[25] Morgans, A. S., and Stow, S. R., 2007. "Model-based control of combustion instabilities in annular combustors". *Combustion and Flame,* **150**(4), pp. 380–399.

[26] Stow, S. R., and Dowling, A. P., 2003. "Modelling of Circumferential Modal Coupling due to Helmholtz resonators". *ASME Turbo Expo*.

[27] Rigas, G., Jamieson, N. P., Li, L. K. B., and Juniper, M. P., 2016. "Experimental sensitivity analysis and control of thermoacoustic systems". *Journal of Fluid Mechanics,* **787**, pp. R1 1–11.

[28] Jamieson, N. P., Rigas, G., and Juniper, M. P., 2017. "Experimental sensitivity analysis via a secondary heat source in an oscillating thermoacoustic system". *International Journal of Spray and Combustion Dynamics,* **0**(0), mar, pp. 1–11.

[29] Jamieson, N. P., and Juniper, M. P., 2017. "Experimental Sensitivity Analysis and the Equivalence of Pulsed Forcing and Feedback Control in Thermoacoustic Systems". *ASME Turbo Expo*, pp. GT2017–63441.